Research Square

Preprints are preliminary reports that have not undergone peer review. They should not be considered conclusive, used to inform clinical practice, or referenced by the media as validated information.

High-resolution imaging of autophagosome formation by LC3 and ATG12 in cells using scanning electron-assisted dielectric microscopy

Tomoko Okada
National Institute of Advanced Industrial Science and Technology

Toshihiko Ogura (t-ogura@aist.go.jp)
National Institute of Advanced Industrial and Technology (AIST) https://orcid.org/0000-0001-8953-6562

Research article

Keywords: Autophagy, scanning electron microscopy, dielectric microscopy, LC3, Atg12, actin, gold colloid

Posted Date: February 7th, 2020

DOI: https://doi.org/10.21203/rs.2.22874/v1

License: This work is licensed under a Creative Commons Attribution 4.0 International License. Read Full License

Abstract

Background

Autophagy is an intracellular self-eating system that plays a central role in cellular recycling. The formation of functional autophagosomes depends on several autophagy- related proteins, including LC3 and Atg12. To analyse an autophagy system, it is essential to precisely examine the cellular functions of cells in liquid condition. For this purpose, we have developed a novel scanning electron-assisted dielectric microscope (SE-ADM) for nanoscale observations of intact cells in aqueous conditions.

Results

Here, we first show that our SE-ADM system observes LC3- and Atg12-containing autophagosomes in cells labelled with antibody-binding gold nano-colloids in medium. We observe that during autophagosome formation, Atg12 localises along the actin mesh structure, whereas LC3 forms arcuate or circular alignments. Our system also detects the different distribution properties of LC3 and Atg12. Atg12 is broadly distributed, whereas LC3 is localised over a smaller range. These differences in spatial-distribution manifest as differently sized spots on fluorescence optical microscopy.

Conclusion

The direct SE-ADM observations of living cells incubated with nanoparticles in a medium may be useful for analysing various cell functions.

Background

Autophagy is a process of self-eating of protein aggregates, damaged organelles and invasive bacteria [1–3]. Cytoplasmic constituents are enclosed by a double-membraned autophagosome, which fuses with the lysosome [2–4]. The formation of functional autophagosomes depends on the hierarchically ordered activity of many autophagy- related proteins [5, 6]. One category of these proteins includes the ubiquitin-like proteins of the LC3 family [7, 8] and conserved Atg12 [9, 10]. When autophagy is induced, LC3 is conjugated to phosphatidyl-ethanolamine at the autophagosome-forming site [8, 10]. This conjugate plays crucial roles in controlling the membrane dynamics and recruiting substrate[10]. Meanwhile, Atg12 is constitutively conjugated to Atg5 [10–12]. As observed by immune-fluorescence microscopy and electron microscopy, the Atg12–Atg5 conjugate is necessary for LC3 lipidation and therefore, essential for autophagosome formation [7, 13–17]. Studies have demonstrated that autophagosomes are constructed through the co-relationship between LC3 and Atg12 [13–17]. To analyse an autophagy system, the functions of autophagic cells must be precisely examined in a medium.

In a recent study, we developed a novel imaging technology named scanning electron-assisted dielectric microscopy (SE-ADM), which enables the observation of intact cells, bacteria and protein particles in water with extremely low radiation damage and without requiring staining and fixation [18, 19]. Our

system can produce high-contrast images of untreated biological specimens in aqueous conditions [19–22]. The biological samples are enclosed in a liquid holder composed of tungsten (W)-coated silicon nitride (SiN) film. Being protected from the electron beam, they are minimally exposed to electron-radiation damage (Supplementary Fig. S1) [19]. Previously, we clearly observed the unstained actin mesh structure in cells under medium conditions using the SE-ADM system [22].

In this report, we newly show that our SE-ADM system observes autophagosomes in cells labelled with antibody-binding gold nano-colloids in medium. Moreover, we revealed the different distribution properties of autophagy related proteins. Our SE-ADM system can directly image the autophagosomes while revealing their intracellular structures in the cells.

Results

To examine LC3 expression and actin structure in rat embryonic fibroblast (REF) [23] cells, we observed fluorescence images of double-stained REF cells labelled with antibodies targeting LC3 and actin (Figs. 1 and 2). The cells were stained by anti-LC3 and anti-actin antibodies tagged with receptive fluorescent secondary antibodies after fixation and permeabilization. The nucleus of the doubly stained cells was clearly visible. Meanwhile, the autophagosomes including LC3 and actin structure were clarified in fluorescent OM images of the double-stained cells (Fig. 1A and B, respectively). In the LC3 fluorescent image, spherical spots with diameter around 1 ∝m are dispersed around the nucleus (Fig. 1A). The actin fluorescence image shows mesh-like structures near the nucleus, and filament structures in the peripheral region (Fig. 1B). When the LC3 and actin fluorescence images are merged, the LC3 is seen to co-localise with the actin mesh-like structure (Fig. 1C). Panels D and E of Fig. 1 are enlarged images of the regions indicated by yellow arrows in Fig. 1C. Conversely, the actin filaments region did not co-localise with LC3 (see panels F and G of Fig. 1, which are enlarged images of the regions indicated by the white arrows in Fig. 1C). Similarly, we observed no co-localisation of LC3 and the phalloidin-labelled actin filaments (Fig. 1H–L).

Next, we examined the localisation of Atg12 and actin filaments by double-stained fluorescence imaging. The FITC-labelled Atg12 proteins were dispersed near the nucleus region as small spots with diameters far below 1 ∝m (Fig. 2A). In contrast, the phalloidin-stained actin filaments were localised in the peripheral region (Fig. 2B). As confirmed in the merged image (Fig. 2C) and the enlarged images of the regions indicated by yellow arrows (Fig. 2D–E) and white arrows (Fig. 2F–G) in Fig. 2C, the Atg12 and actin filaments were not co-localised. Furthermore, the Atg12 fluorescence spots were much smaller than the LC3 fluorescence spots (Fig. 2H and I).

Our new SE-ADM imaging technology is schematised in Supplementary Fig. S1. REF cells or mouse breast cancer cells (4T1E/M3) were cultured on silicon nitride (SiN) film placed in the aluminium holder under a handmade culture dish [20]. After 4–5 days of culture, the cells formed a confluent monolayer on the SiN film. After 2–3 hours of starvation, the aluminium holder with the cells on SiN film was detached and sealed by another acrylic plate, and then introduced to the SE-ADM system [19, 20]. Prior to

observation, the cells were fixed with 4% paraformaldehyde, permeabilised with 0.2% Tween 20, and labelled with anti-LC3 antibody and 60-nm gold colloids conjugated to a secondary antibody. Figure 3 shows an SE-ADM image of the labelled cells. Figure 3A clearly reveals the vesicles and part of the nucleus at the left. The LC3 bound with 60 nm-diameter gold colloids formed an arcuate line near the nucleus (Fig. 3A). This arc-like structure is clarified in the enlarged image (Fig. 3B), pseudo-colour map (Fig. 3C) and 3D pseudo-colour map (Fig. 3D). Arcuate lines also appeared in other cell regions (see Supplementary Fig. S2A and the enlarged images Fig. 3E–G of the REF cells, and the circularly aligned gold colloids in Supplementary Fig. S2B and the enlarged images Fig. 3H–J of the 4T1E/M3 cells). These alignments correspond to the reported structures of LC3 localisation [3, 4].

To clarify the localisation of Atg12 and F-actin involved in autophagosome formation, we explored the Atg12 distribution in the cells using the SE-ADM system (Fig. 4). We observed the dielectric SE-ADM images of cells labelled with anti-Atg12 antibody and 60-nm gold colloid-conjugated second antibody. Figure 4A is a low-magnification image (1,500×) showing the nucleus, and Fig. 4B is a high-magnification image (10,000×) of the area enclosed by the red square in Fig. 4A, focussing on the mesh-like-structure near the nucleus. In previous reports, we stained the cells with anti-actin antibody and gold colloid-conjugated with secondary antibody. Under the SE-ADM system, the mesh-like structure was confirmed to be actin [22]. For a detailed analysis, we further enlarged the region close to the nucleus (enclosed within the red square in Fig. 4B), obtaining Fig. 4C. A pseudo-colour map (Fig. 4D) was then obtained by intensity inversion of Fig. 4C. In Panels D and E of Fig. 4, the Atg12 labelled with 60-nm gold colloids is clearly lined along the actin mesh-like structures. Furthermore, the 3D pseudo-colour map clarifies where the gold colloids localise (Fig. 4F). The same results were obtained in another cell region (Supplementary Fig. S3). These results suggested that Atg12 interacts with actin mesh structures near the nucleus, consistent with some previous reports [3].

The gold colloids bound to LC3 were adjacently arranged (Fig. 3D, G and J), whereas those bound to Atg12 were distributed more widely (Fig. 4F). The different distributions of the gold colloids bound to LC3 and Atg12 are exhibited in the histograms of minimal intervals of the gold colloids (Fig. 4G). The intervals between gold colloids bound to LC3 were usually within 400 nm, and sharply peaked at 150 nm. On the other hand, the minimal intervals between the Atg12-bound colloids covered a broad range (100–1100 nm) with a low peak at 500 nm (Fig. 4G).

Discussion

Autophagy is a catabolic process that degrades cytoplasmic components for recycling [1, 2]. Recent findings suggested that autophagosome formation is mediated and controlled by actin-nucleation promoting proteins [3, 16, 24]. Actin is essential in a number of cellular processes such as motility, exocytosis and endocytosis, and autophagy [24]. Filamentous actin (F-actin) is composed of globular actin (G-actin) subunits that are assembled and disassembled by a wide variety of proteins [25]. Actin assemblage and autophagy are considered to co-occur [3, 16, 24], and a reciprocal interconnection seems to operate between autophagy and actin assembly [3, 16, 24].

The spatial resolution of our SE-ADM system is 8 nm [19]. Our system produces high-contrast images of untreated biological specimens in aqueous conditions. In our previous report, the SE-ADM system clearly revealed the actin-mesh structures in mammalian cells under aqueous conditions [22].

Here, we analysed the relationship between the autophagy-related proteins and actin using our newly developed SE-ADM system. The autophagy-related protein Atg12 was clearly localised on the actin mesh-like structure (Fig. 4C–E, Supplementary Fig. S3). The Atg12 was widely dispersed as small dots in the actin mesh area. In contrast, the 60-nm gold colloids bound to the LC3 proteins were arranged in an arcuate (Fig. 3D and G) or circular (Fig. 3H–J) formation near the nucleus. Our results suggest that autophagosome formation involving LC3 and Atg12 is correlated with actin nucleation (Fig. 4H). Previous studies have similarly demonstrated that autophagosome formation is assisted by actin nucleation with LC3 and Atg12 [3]. Here, we directly observed the relationship between autophagosome formation and actin/LC3 or actin/Atg12 in liquid conditions using our high-resolution imaging system (SE-ADM).

The spatial resolution of general fluorescence OM is limited to a few hundred nanometers. Therefore, precise and direct observations of the autophagosomes associated with LC3 and Atg12 are precluded by this method (Figs. 1 and 2). In contrast, the high-resolution SE-ADM system clearly observed the inner cell structure labelled with 60-nm gold colloids (Figs. 3 and 4), and revealed the different localisation properties of LC3 and Atg12. The minimal intervals between the gold colloids bound to LC3 were typically around 150 nm, and most of the higher intervals were below 400 nm (Fig. 4G). In the fluorescence OM image of LC3, this dense distribution manifested as large spots with diameters around 1 ∝m (Fig. 2H). In contrast, the gold colloids bound to Atg12 were broadly distributed with many long intervals (100–1100 nm; see Fig. 4G), so the fluorescent spots were very small (far below 1 ∝m in diameter; Fig. 2I). Accordingly, our SE-ADM system is more suitable for detailed analyses in living cells than the OM system.

Conclusions

We analysed the relationship between two autophagy-related proteins (LC3 and Atg12) and the actin structure of cells in liquid conditions using our newly developed SE-ADM system. We revealed that during autophagosome formation, Atg12 localises along the actin mesh-like structure, while LC3 forms arcuate or circular alignments. Our results suggest that autophagosome formation involving LC3 and Atg12 is closely related to actin nucleation. Moreover, our system successfully revealed the different distribution properties of LC3 and Atg12. Other membrane proteins in intact cells under medium conditions are also observable by our methods.

Materials And Methods

Liquid sample and culture dish holders

The liquid sample holder was formed as previously described [21]. Briefly, the liquid sample holder comprised an upper Al holder and a lower acrylic resin portion that maintained the sample solution at

atmospheric pressure between the SiN films [19, 20]. A 50 nm-thick SiN film supported by a (0.4 × 0.4) mm^2 window in a Si frame ((4 × 4) mm^2, 0.381 mm thickness; Silson Ltd., Warwickshire, UK) was coated with tungsten (W) using a magnetron sputtering device (Model MSP-30T, Vacuum Device Inc., Ibaraki, Japan), as previously described [19, 20]. The upper W-coated SiN film was attached to the Al holder with double-sided tape, and the W layer on the SiN film was connected to the Al holder with silver conductive ink. A handmade Al holder with a Si frame was attached beneath a 35-mm culture dish adhered with double-sided tape to a square hole in the centre of the dish, as previously described [20, 21]. The culture dish holder was subsequently UV-sterilised for 17–18 h.

Sample preparation of 4T1E/M3 cells and rat embryo fibroblasts (REF)

Mouse breast cancer cells (4T1E/M3) were established as previously described [26–28]. The cells were cultured in high-glucose RPMI-1640 medium (Wako, Osaka, Japan) containing 10% fetal calf serum (FCS, invtrogen) and 20 mM HEPES at 37 °C under 5% CO_2. The medium (1.5 mL/dish) was poured into a culture dish attached to the 50-nm SiN–Al holder. The cells (~ 4×10^4; 20 μL/dish) were seeded and cultured at 37 °C under 5% CO_2. The medium was changed after 2–3 days. After 4–5 days, the cells had formed a sub-confluent or completely confluent monolayer on the SiN membrane in the holder [20].

The REF cells [23], kindly provided by Dr. Keisuke Ohta (Kurume University School of Medicine), were cultured in low-glucose D-MEM medium (Wako) containing 10% fetal calf serum (FCS), 20 mM HEPES and L-glutamine at 37 °C under 5% CO_2. The cells (~ 4×10^4; 20 μL/dish) were seeded and cultured in 1.5 ml medium as described for the 4T1E/M3 cells. Again, the medium was changed after 2–3 days, and the cells formed a sub-confluent or completely confluent monolayer on the SiN membrane in the holder after 4–5 days [20].

Before the immunolabelling, cells were cultured for 2 hours with the medium without serum at 37 °C under 5% CO_2 for starvation to induce autophagy.

Immunofluorescence staining of the cells and observation by optical microscopy

The 4T1E/ME or REF cells cultured in a 35-mm glass-bottom dish (Matsunami Glass Ind., Ltd., Osaka, Japan) were starved and fixed with 4% paraformaldehyde containing PBS for 10 min at room temperature (r.t.), washed twice, and permeabilised in 0.2% Tween 20 for 30 min at r.t.

For double fluorescence staining of LC3 and F-actin, the fixed and permeabilised cells in the glass-bottom dishes were stained with mouse anti-LC3 antibody (Medical & Biological Laboratories Co. Ltd. Cat#:M152-3, Clone 4E12, 1/50) diluted in PBS for 30 min at r.t., washed twice, and stained with FITC-conjugated anti-mouse IgG antibody (Code 55522, MP Biomedicals Inc., Auroa, Ohio, 1/100) for 30 min at r.t. The cells were then stained with rabbit anti-mouse F-actin antibody (Bioss Inc., Massachusetts, USA, Cat #: bs-1571R, 1/100) for 30 min at r.t., washed twice, and stained with anti-rabbit IgG-conjugated rhodamine (Jackson Immunoresearch Laboratory Inc., Pennsylvania, USA, Cat # 711-065-152, 1/100) for 30 min at r.t. For phalloidin staining, cells were stained with the alexa fluor 568 phalloidin (Thermo Fisher,

A12380, 1/300) for 30 min at r.t. instead of anti-mouse F-actin and the second antibody. After washing twice, the dish was observed under a fluorescence optical microscope (AXIO Observer A1; CarlZeiss, Oberkochen, Germany). The fluorescence images of the cells were acquired through fluorescence filters at excitation/emission wavelengths of 480/520 nm (green fluorescence of FITC) or 565/620 nm (red florescence of Alexa Fluor or rhodamine).

For double fluorescence staining of Atg12 and F-actin, the fixed and permeabilised cells in the glass-bottom dishes were stained with rabbit anti-Atg12 antibody (GNT, Cat#:GTX124181, 1/50) diluted with PBS for 30 min at r.t., washed twice, and stained with FITC-conjugated anti-rabbit IgG (Code:55662, MP Biomedicals Inc, 1/100) for 30 min at r.t. The cells were then stained with Alexa Fluor 568 phalloidin (Thermo Fisher, A12380, 1/300) for 30 min at r.t. After two washes, the dish was observed under a fluorescence optical microscope (AXIO Observer A1; CarlZeiss, Oberkochen, Germany). Fluorescence images of the cells were acquired under the filtering conditions described for doubly stained LC3 and F-actin.

Immunolabelling of cells using antibody and 60-nm gold colloids

The cells seeded in the dish holder on the 50-nm SiN film were starved and fixed with 4% paraformaldehyde diluted with PBS for 10 min at r.t., washed twice with PBS, and permeabilised in 0.2% Tween 20 for 30 min at r.t. The cells were stained by mouse anti-LC3 antibody (MBL, Cat#: M152-3, 1/50) for 30 min at r.t., washed twice with PBS, and stained with anti-mouse IgG-conjugated 60-nm gold colloids (Cytodiagnostics Inc. Ontario, Canada, catalogue # AC-60-02-05, 1/50) for 30 min at r.t. After two washes, the holder was attached to the acrylic sample holder on the 50-nm SiN film and observed with the SE-ADM system [20, 21].

For 60-nm gold labelling of Atg12, the cells were fixed, permeabilised and stained with rabbit anti-Atg12 antibody (GNT, Cat# GTX124181, 1/50) for 30 min at r.t., washed twice with PBS, and stained with anti-rabbit IgG-conjugated 60-nm gold colloids (Cytodiagnostics Inc. Ontario, Canada, catalogue #: AC-60-17, 1/50) for 30 min at r.t.

High-resolution SE-ADM system and FE-SEM setup

The high-resolution SE-ADM imaging system is based on FE-SEM (JSM-7000F, JEOL, Tokyo, Japan), and is shown in Supplementary Fig. S1. The liquid sample holder was mounted onto the SEM stage, and the detector terminal was connected to a pre-amplifier under the holder[19]. The electrical signal from the pre-amplifier was passed through a low-pass filter and fed into the AD converter (AIO-163202FX-USB, Contec Co. Ltd., Osaka, Japan) as previously described [19]. The low-pass filtered (LPF) and electron beam-scanned signals were logged in a PC through an AD converter at a sampling frequency of 50 kHz. SEM images (1,280 × 1,020 pixels) were captured under 1,000–20,000 × magnification with a scanning time of 80 s, a working distance of 7 mm, an EB acceleration voltage of 4–8 kV, and a current of 10 pA.

Image processing

The SE-ADM signal data from the AD converter were transferred to a personal computer (Intel Core i7, 2.8 GHz, Windows 7). The LPF and scanned signals were processed into high-resolution SE-ADM images using the image-processing toolbox of MATLAB R2014a (Math Works Inc., Natick, MA, USA). The original SE-ADM images were filtered through a 2D Gaussian filter (GF) with a kernel size of (11 × 11) pixels and a radius of 1.2σ. The background was removed by subtracting the SE-ADM images from the filtered images using a broad GF (400 × 400 pixels, 200σ).

Calculation of minimum interval between gold colloids

To calculate the minimal intervals between pairs of gold colloids, we randomly selected 283 and 300 colloids from the SE-ADM images of cells stained with anti-LC3 antibody (4 images) and anti-Atg12 antibody (3 images), respectively. The minimal interval between the gold colloids was calculated as the minimum distance between the (x, y) coordinates of the working gold colloid in the image and the (x, y) coordinates of the other colloids. The calculation was performed in MATLAB R2014a (Math Works Inc., Natick, MA, USA) running on a PC (Intel Core i7, 3.2 GHz, Windows 7).

Supplementary Information

Additional file 1: Figure S1. Overview of autophagosome observations in cells using the SE-ADM system. Figure S2. SE-ADM images of EM3 cells stained with anti-LC3 antibody conjugated with 60-nm gold colloids. Figure S3. SE-ADM images of REF cells stained with anti-Atg12 antibody conjugated with 60-nm gold colloids.

Declarations

Acknowledgements

We thank Ms. Yoko Ezaki and Ms. Miho Iida for their excellent technical assistances. We thank Dr. Keisuke Ohta (Kurume University School of Medicine) for kindly providing REF cells.

Authors' Contributions

T. Okada and T. Ogura performed and designed the research. T. Ogura designed and developed the SE-ADM system and culture dish holder. All authors contributed to observing the experimental data, discussing the experimental results and writing the manuscript. All authors read and approved the final manuscript.

Funding

This study was supported by JSPS KAKENHI grant numbers JP19H03230, JP19H05568, and supported by JST CREST grant number JPMJCR19H2. The funding body did not participate in the conception of the study, the collection, analysis and interpretation of the data or in the preparation of the manuscript.

Availability of data materials

All data generated or analyzed during this study are included in this published article.

Ethics approval and consent to participate

Not Applicable.

Consent for publication

Not Applicable.

Competing interests

The authors declare that they have no competing interests.

References

1. Mizushima N. Autophagy: process and function. Gene Dev. 2007; 21:2861–73.
2. Mizushima N, Levine B, Cuervo AM, Klionsky DJ. Autophagy fights disease through cellular self-digestion. Nature. 2008; 451:1069–75.
3. Coutts AS, La Thangue NB. Regulation of actin nucleation and autophagosome formation. Cell Mol Life Sci. 2016; 73:3249–63.
4. Demarchi F, Bertoli C, Copetti T, Tanida I, Brancolini C, Eskelinen EL, Schneider C. Calpain is required for macroautophagy in mammalian cells. J Cell Biol. 2006; 175(4):595–605.
5. Xie Z, Klionsky DJ. Autophagosome formation: Core machinery and adaptations. Nat Cell Biol. 2007; 9(10):1102–9.
6. Boya P, Reggiori F, Codogno P. Emerging regulation and functions of autophagy. Nat Cell Biol. 2013; 15(7):713–20.
7. Kabeya Y, Mizushima N, Yamamoto A, Oshitani-Okamoto S, Ohsumi Y, Yoshimori T. LC3, GABARAP and GATE16 localize to autophagosomal membrane depending on form-II formation. J Cell Sci. 2004; 117:2805–12.
8. Tanida I, Ueno T, Kominami E. LC3 conjugation system in mammalian autophagy. Int J Biochem Cell B. 2004; 36(12):2503–18.
9. Mizushima N, Sugita H, Yoshimori T, Ohsumi Y. A new protein conjugation system in human - The counterpart of the yeast Apg12p conjugation system essential for autophagy. J Biol Chem. 1998; 273(51):33889–92.
10. Geng J, Klionsky DJ. The Atg8 and Atg12 ubiquitin-like conjugation systems in macroautophagy. EMBO Rep. 2008; 9(9):859–64.
11. Jounai N, Takeshita F, Kobiyama K, Sawano A, Miyawaki A, Xin KQ, Ishii KJ, Kawaii T, Akira S, Suzuki K *et al*. The Atg5-Atg12 conjugate associates with innate antiviral immune responses. Proc Natl Acad

Sci USA. 2007; 104(35):14050–5.

12. Otomo C, Metlagel Z, Takaesu G, Otomo T. Structure of the human ATG12 similar to ATG5 conjugate required for LC3 lipidation in autophagy. Nat Struct Mol Biol. 2013; 20(1):59–66.
13. Rubinstein AD, Eisenstein M, Ber Y, Bialik S, Kimchi A. The autophagy protein Atg12 associates with antiapoptotic Bcl-2 family members to promote mitochondrial apoptosis. Mol Cell. 2011; 44:698–709.
14. Dooley HC, Razi M, Polson HEJ, Girardin SE, Wilson MI, Tooze SA. WIPI2 links LC3 conjugation with PI3P, autophagosome formation, and pathogen clearance by recruiting Atg12-5-16L1. Mol Cell. 2014; 55:238–52.
15. Biazik J, Vihinen H, Anwar T, Jokitalo E, Eskelinen EL. The versatile electron microscope: An ultrastructural overview of autophagy. Methods. 2015; 75:44–53.
16. Coutts AS, La Thangue NB. Actin nucleation by WH2 domains at the autophagosome. Nat Commun. 2015; 6:7888.
17. Ligeon LA, Barois N, Werkmeister E, Bongiovanni A, Lafont F. Structured illumination microscopy and correlative microscopy to study autophagy. Methods. 2015; 75:61–8.
18. Ogura T. Direct observation of unstained biological specimens in water by the frequency transmission electric-field method using SEM. PloS ONE. 2014; 9(3):e92780.
19. Ogura T. Nanoscale analysis of unstained biological specimens in water without radiation damage using high-resolution frequency transmission electric-field system based on FE-SEM. Biochem Bioph Res Commun. 2015; 459:521–8.
20. Okada T, Ogura T. Nanoscale imaging of untreated mammalian cells in a medium with low radiation damage using scanning electron-assisted dielectric microscopy. Sci Rep. 2016; 6:29169.
21. Okada T, Ogura T. High-resolution imaging of living mammalian cells bound by nanobeads-connected antibodies in a medium using scanning electron-assisted dielectric microscopy. Sci Rep. 2017; 7:43025.
22. Okada T, Ogura T. Nanoscale imaging of the adhesion core including integrin beta 1 on intact living cells using scanning electron-assisted dielectric-impedance microscopy. PloS ONE. 2018; 13:e0204133.
23. Land H, Parada LF, Weinberg RA. Tumorigenic conversion of primary embryo fibroblasts requires at least two cooperating oncogenes. Nature. 1983; 304:596–602.
24. Kast DJ, Dominguez R. The cytoskeleton-autophagy connection. Curr Biol. 2017; 27:R318–R26.
25. Machaidze G, Sokoll A, Shimada A, Lustig A, Mazur A, Wittinghofer A, Aebi U, Mannherz HG. Actin filament bundling and different nucleating effects of mouse diaphanous-related formin FH2 domains on Actin/ADF and Actin/Cofilin complexes. J Mol Biol. 2010; 403:529–45.
26. Takahashi M, Furihata M, Akimitsu N, Watanabe M, Kaul S, Yumoto N, Okada T. A highly bone marrow metastatic murine breast cancer model established through in vivo selection exhibits

enhanced anchorage-independent growth and cell migration mediated by ICAM-1. Clin Exp Metastas. 2008; 25:517–29.

27. Takahashi M, Miyazaki H, Furihata M, Sakai H, Konakahara T, Watanabe M, Okada T. Chemokine CCL2/MCP-1 negatively regulates metastasis in a highly bone marrow-metastatic mouse breast cancer model. Clin Exp Metastas. 2009; 26:817–28.
28. Sakai H, Furihata M, Matsuda C, Takahashi M, Miyazaki H, Konakahara T, Imamura T, Okada T. Augmented autocrine bone morphogenic protein (BMP) 7 signaling increases the metastatic potential of mouse breast cancer cells. Clin Exp Metastas. 2012; 29:327–38.

Figures

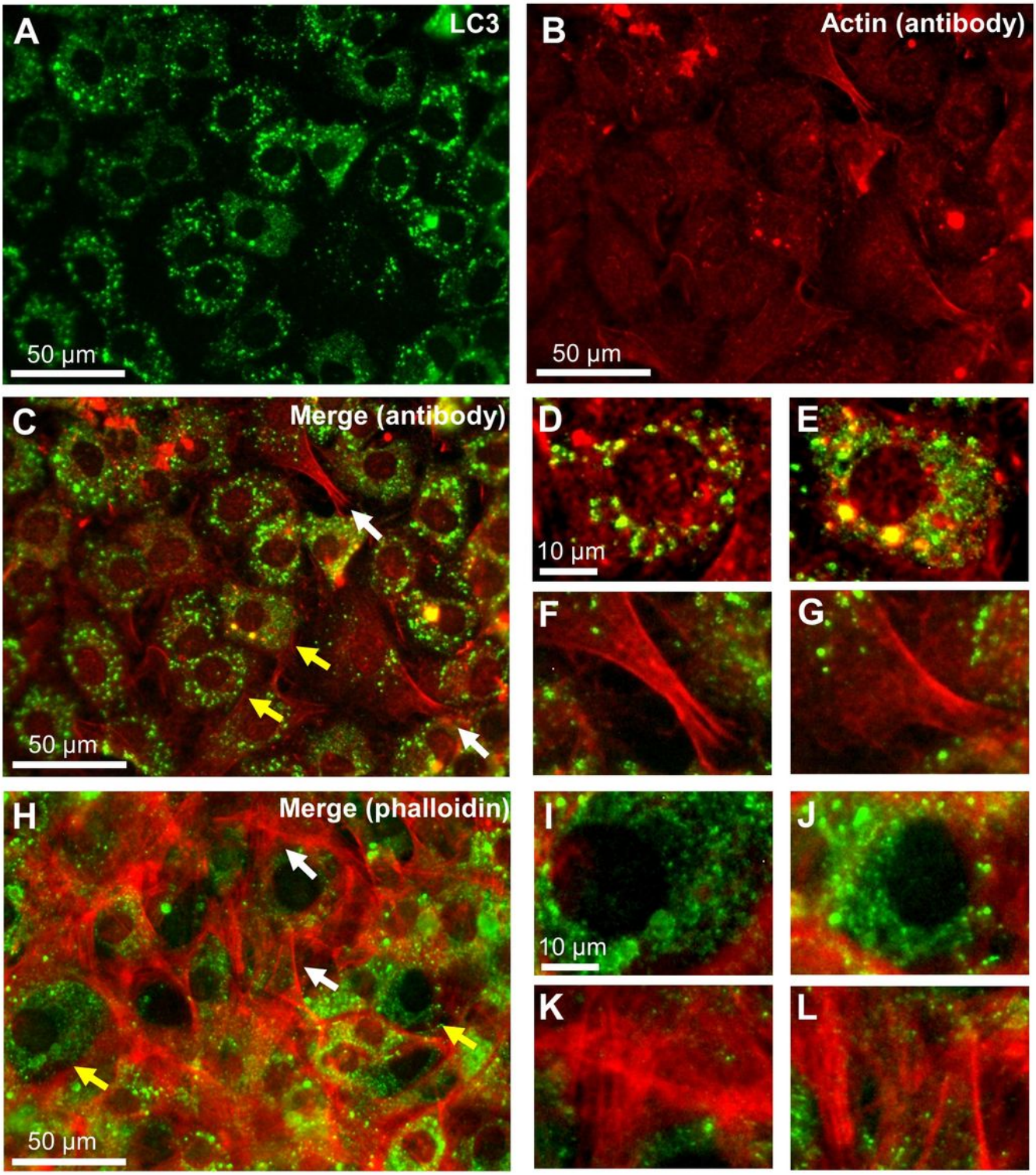

Figure 1

Observation of LC3 and actin double-stained fluorescence images of REF cells. (A) Fluorescence image of anti-LC3 and FITC-immunostained cells under optical microscope (OM) with a green fluorescence filter (400× magnification). The LC3 and actin in the REF cells were doubly stained by fluorescence imunnolabelling. (B) Fluorescence image of actin stained with anti-actin antibody and rhodamine, viewed through a red fluorescence filter (400× magnification). (C) Merged fluorescence image of LC3 and actin.

(D, E) Enlarged images of the LC3-rich areas (pointed by yellow arrows in C). LC3 was localised along the actin mesh structures near the nucleus. (F, G) Enlarged images of the LC3-poor areas (pointed by white arrows in C), showing many actin filament bundles. (H) Merged image of LC3 and phalloidin-labelled actin. (I, J) Enlarged images of the LC3-rich areas (pointed by yellow arrows in H). (K, L) Enlarged images of the LC3-poor areas (pointed by white arrows in H). Scale bars: 50 μm in (A–C, H), 10 μm in (D, I).

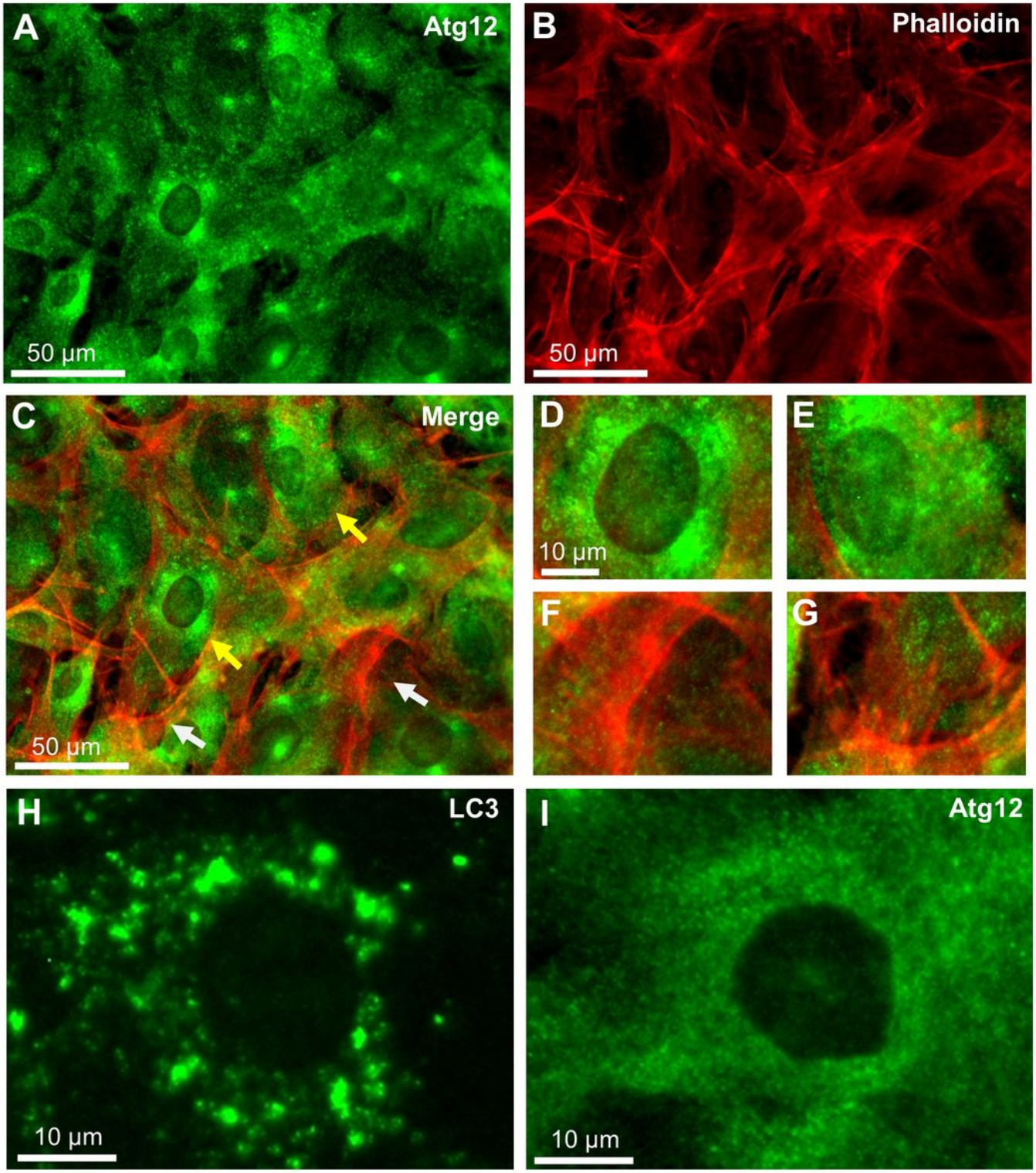

Figure 2

Observation of ATG12 and actin double-stained fluorescence images of REF cells. (A) Fluorescence image of anti-Atg12 and FITC-immunostained cells under OM with a green fluorescence filter (400× magnification). The Atg12 and actin in the REF cells were doubly stained by fluorescence imunnolabelling. The small fluorescence spots near the nucleus are Atg12. (B) Fluorescence image of actin filament stained by rhodamine conjugated phalloidin, viewed through a red fluorescence filter (400× magnification). (C) Merged fluorescence image of Atg12 and actin. (D, E) Enlarged images of the Atg12-rich areas (pointed by yellow arrows in C). Atg12 was localised near the nucleus where filamentous actin was absent. (F, G) Enlarged images of the Atg12-poor areas (pointed by white arrows in C). Fluorescence spots of Atg12 are rare in the filamentous actin area. (H, I) Enlarged images of the LC3 and Atg12 fluorescence spots, respectively. The Atg12 spots are much smaller than the LC3 spots. Scale bars: 50 μm in (A–C), 10 μm in (D, H, I).

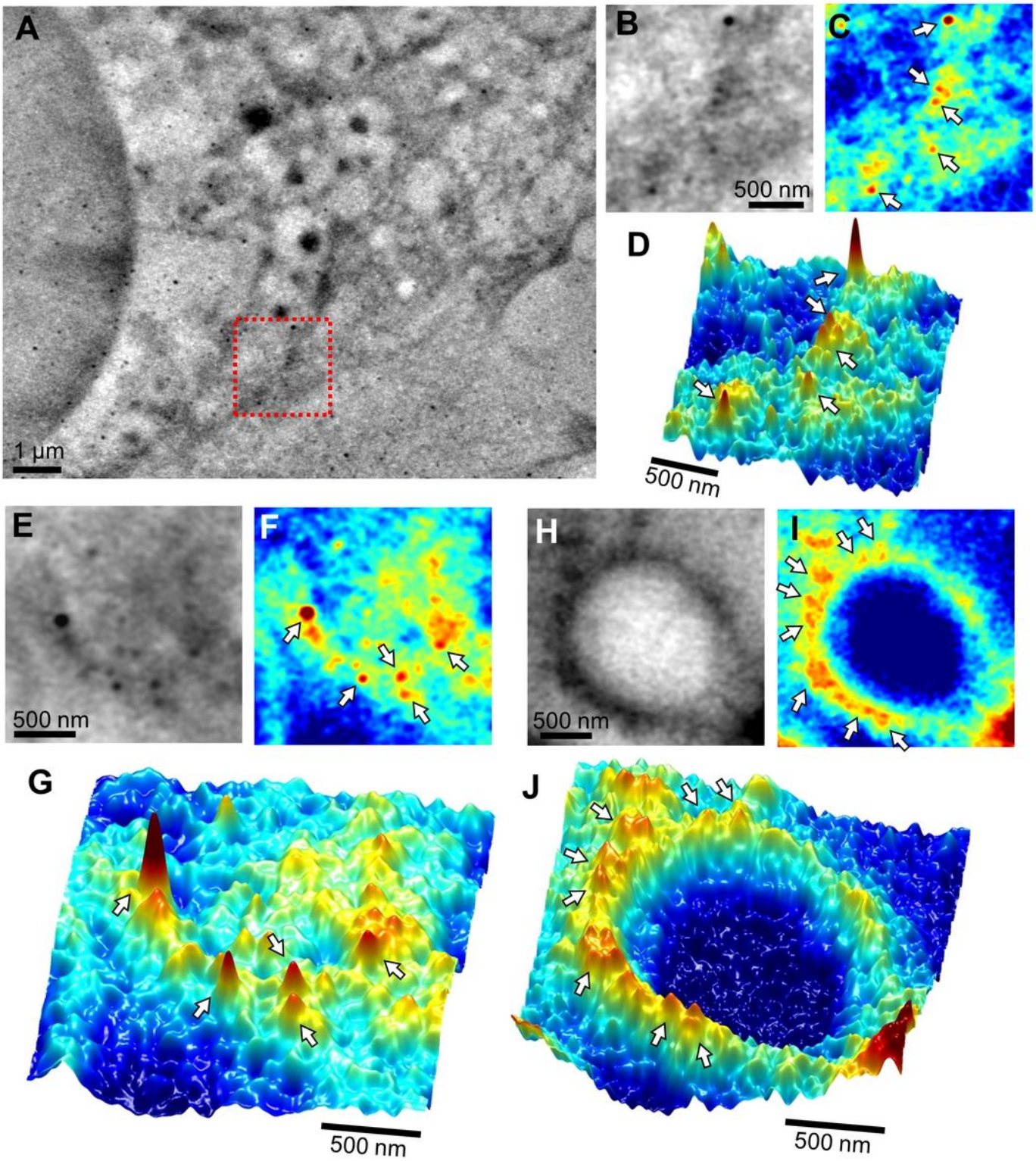

Figure 3

Dielectric images of REF and EM3 cells stained with anti-LC3 antibody conjugated with 60-nm gold colloids. (A) Dielectric images of REF cells stained with anti-LC3 antibody and 60-nm gold colloids after paraformaldehyde fixation and 0.1% Tween-20 permeabilisation (5,000× magnification, 6 kV electron beam). (B) Enlarged image of the red boxed area in (A), showing LC3 bound to 60-nm gold colloids. LC3 is aligned in an arc-like formation. (C) Pseudo-colour map of (B) after intensity inversion. (D) 3D colour

map of (C). (E) Enlarged image of the red boxed area in Supplementary Fig. 2A. (F) Pseudo-colour map of (E) after intensity inversion. (G) 3D colour map of (F). LC3 is aligned in an arcuate formation. (H) Dielectric images of 4T1E/M3 cells stained with anti-LC3 antibody and 60-nm gold colloids after paraformaldehyde fixation and 0.1% Tween-20 permeabilisation. Enlarged image of red boxed area in supplementary Fig. 2B. (I) Pseudo-colour map of (H) after intensity inversion. LC3 aligns in a circular formation. (J) 3D colour map of (I). Scale bars: 1 μm in (A), 500 nm in (B, D, E, H, G, J).

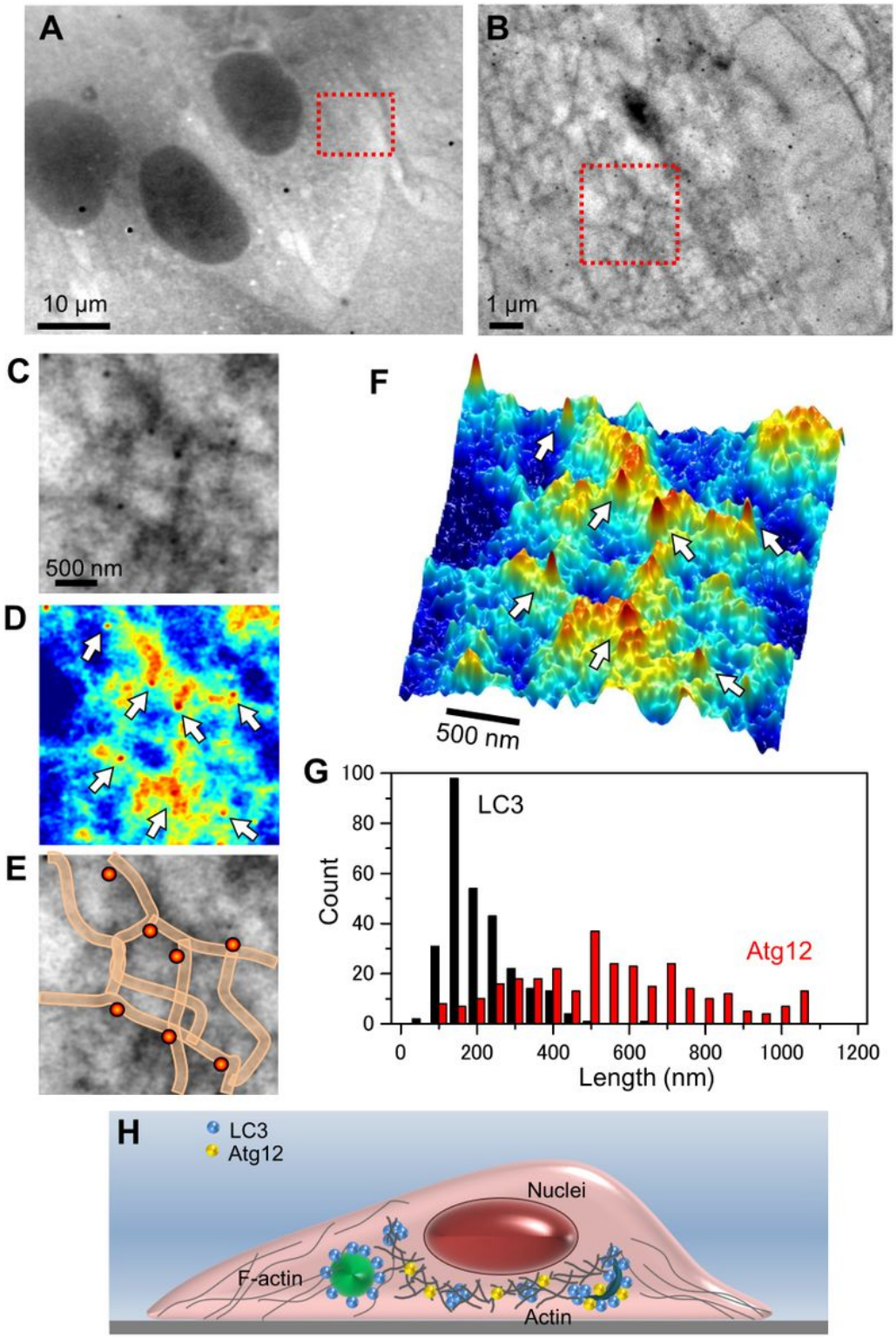

Figure 4

Dielectric images of REF cells stained with anti-Atg12 antibody conjugated with 60-nm gold colloids. (A) Low-magnification dielectric image of REF cells stained with anti-Atg12 antibody and 60-nm gold colloids after paraformaldehyde fixation and 0.1% Tween-20 permeabilisation (1,500× magnification, 6 kV electron beam). (B) High-magnification image (10,000×) of the red boxed area in (A), showing Atg12 bound with 60-nm gold colloids. Atg12 is dispersed over the whole area near the nucleus. (C) Enlarged image of the red boxed area in (B). Atg12 is localised along the mesh structure. (D) Pseudo-colour map of (C) after intensity inversion. (E) Schematic diagram of mesh-like structures and gold colloids superimposed on a dielectric image of (C). (F) 3D colour map of (D). (G) Histograms of minimum intervals between pairs of gold colloids. Minimum intervals between LC3-bound colloids are small and sharply peaked, whereas those between Atg12 are larger and broadly distributed. (H) A schematic picture of structural organisation of autophagosomes involving LC3 and Atg12 with actin. Atg12 is dispersed as small particles near the nucleus. LC3 is arranged into arcuate or circular structures. Scale bars: 10 μm in (A), 1 μm in (B), 500 nm in (C, F).

Supplementary Files

This is a list of supplementary files associated with this preprint. Click to download.

- SuppleSEADMautophagyBMCmol200121a.docx